

# A mechanistic study of nonlinear solute transport in a groundwater–surface water system under steady state and transient hydraulic conditions

Michel C. Boufadel

Department of Civil and Environmental Engineering, Temple University, Philadelphia, Pennsylvania

**Abstract.** Two laboratory experiments were conducted to investigate the effects of tides and buoyancy on beach hydraulics in the presence of a seaward groundwater flow due to an elevated “regional” water table. In the first experiment, case 1, the difference in concentration between the salt water at sea and the water of the regional aquifer was small,  $2.4 \text{ g L}^{-1}$ , such that it did not engender density gradients; the salt acts as a tracer in this case. In the second experiment, case 2, the difference was  $\sim 32.0 \text{ g L}^{-1}$ , which creates a significant density gradient. This case corresponds to the presence of fresh groundwater in the subsurface of the coasts of the continental United States. The experiments were numerically simulated by the marine unsaturated (MARUN) model, a numerical model for density-and-viscosity-dependent flows in two-dimensional variably saturated media. The long-term experimental and numerical results showed that the seawater plume entered the beach from the sea and occupied most of the intertidal zone. The maximum depth of the seawater plume was near the midsection of the intertidal zone, and it decreased near the low and high tide lines. When viewed in the context of case 2, these results indicate an inverted salinity distribution in beaches subjected to tides with salt water from sea overtopping the freshwater lens. For both cases, water from the regional aquifer moved seaward beneath the seawater in the intertidal zone and pinched out near the low tide mark. We also noted that beach hydraulics are highly two dimensional with water entering the beach at a near-vertical angle and leaving it at a near-horizontal angle, which casts doubts on analyses of beach hydraulics based on the Dupuit assumption. Findings from this work have direct implications within the practice of bioremediation of oil spills on beaches. We found that applying dissolved nutrients on the beach surface at low tide is superior to applying them in a trench landward of the beach. This is because the residence time of the nutrient plume in the bioremediation zone of the beach in the prior situation is longer than that in the latter.

## 1. Introduction

Bioremediation is an emerging technology for restoration of oil-contaminated beaches [Merlin *et al.*, 1995]. One implementation of bioremediation involves the addition of nutrients, such a nitrogen and phosphorus, to stimulate the growth of indigenous hydrocarbon-degrading bacteria [Venosa *et al.*, 1996]. The effectiveness of biostimulation depends on contact between the added nutrients and the oil-polluted zone, which is usually less than  $\sim 25 \text{ cm}$  below the beach surface [Rosenburg *et al.*, 1992]. Ideally, nutrient concentrations in contact with the oil should be sufficient to support maximal growth rate of the oil-degrading bacteria, and this minimum concentration must be maintained for the longest possible time. Therefore maximizing the residence time of the nutrients in the contaminated zone of the beach is an important goal for bioremediation.

Many approaches have been developed to maintain contact between oil and nutrients, including lipophilic and slow-release methods for the nutrients. However, most slow-release and many lipophilic fertilizers rely on dissolution of the nutrients into the aqueous phase before they can be used by hydrocar-

bon degraders [Safferman, 1991]. Thus design of effective oil bioremediation strategies and nutrient delivery systems requires an understanding of the transport of water-soluble fertilizer in the beach.

Dissolved nutrients are expected to move with the water in the beach sand. Water flow through the porous matrix of a beach is driven by a combination of three main factors: waves, fresh groundwater flow, and tide. Waves operate through the mechanism of run-up–run-down [Riedl *et al.*, 1972; Brown and McLachlan, 1990]. At wave run-up, water enters the beach from above and percolates vertically through the unsaturated zone until it reaches the water table. At wave run-down, water moves in a predominant horizontal direction and exits the beach. The second factor that drives flow through sandy beaches is the flow of fresh groundwater from coastal aquifers. Under steady state hydraulic boundary conditions (i.e., no waves or tide), incoming fresh water floats above a saltwater wedge (due to density difference) and exits the beach [Glover, 1959; Henry, 1964; Frind, 1982; Huyakorn *et al.*, 1987; Galeati *et al.*, 1992]. The saltwater wedge acts as an impermeable boundary for the fresh water, forcing it to cone up toward the beach surface. The funneling effect due to the saltwater wedge causes the seaward velocity of the fresh water to increase when approaching the beach surface. The third factor that influences groundwater flow in beaches is the tide that produces a net

Copyright 2000 by the American Geophysical Union.

Paper number 2000WR900159.  
0043-1397/00/2000WR900159\$09.00

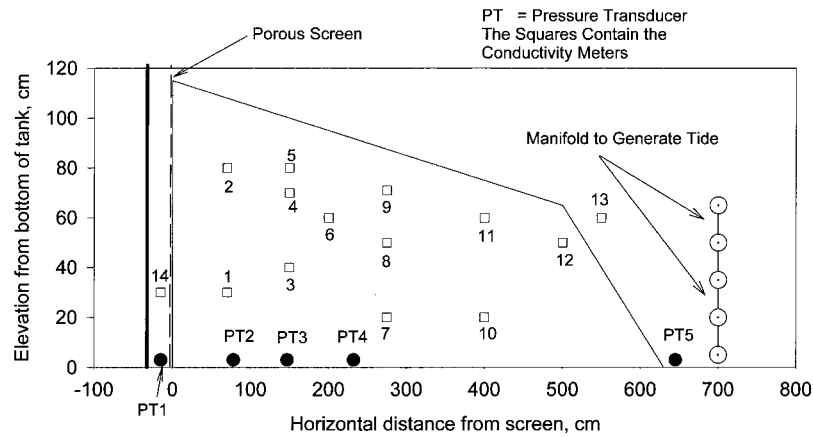


Figure 1. Schematic of the beach and location of sensors.

seaward hydraulic gradient within the beach matrix (averaged over one tidal period) [Philip, 1973; Nielsen, 1990; Boufadel *et al.*, 1998]. The seaward hydraulic gradient is due to the fact that the beach fills much faster than it drains, resulting in an average beach water table that is above mean sea water level.

The effects of buoyancy and tide on beach hydraulics and hydrodynamics (i.e., solute transport) are investigated in this work using a laboratory beach setup and the numerical model MARUN [Boufadel *et al.*, 1997; Boufadel *et al.*, 1999a]. The marine unsaturated (MARUN) model can simulate water flows in the saturated and the unsaturated zones of two-dimensional porous media taking into account the effects of salt concentration on water density and water viscosity. Such flows are designated here as density-and-viscosity-dependent flows in two-dimensional variably saturated media.

The layout of the paper is as follows. First a brief review of prior studies is reported, and then, the governing equations of the MARUN model are presented. A description of the experimental tank is then provided, and two experiments simulating natural beach hydraulics and hydrodynamics are reported. The MARUN model is used to predict water flow and solute transport in these two experiments and to further the understanding of the mechanisms affecting water flow and solute transport in the laboratory beach. The dimensionless formulation of Boufadel *et al.* [1998, 1999a] is used to scale up the laboratory results. Finally, the implications of the results on nutrient transport during bioremediation of oil spills on beaches are discussed.

## 2. Prior Work

The presence of fresh groundwater in a marine environment has been considered by many researchers in the context of saltwater intrusion in aquifers. The earliest solution was presented by W. Ghyben and A. Herzberg [Bear, 1972, p. 559], who assumed that a sharp interface exists between the fresh water and the saltwater wedge beneath it and that both water masses are at hydrostatic equilibrium. Glover [1959] presented a more physically correct solution for the interface by assuming that the two liquids are at dynamic equilibrium. Henry's [1964] analytical solution is even more realistic because it accounts for mechanical dispersion which results in a gradual change of the salinity between the two water masses. Frind [1982] presented a finite element solution using a velocity-dependent dispersion

coefficient and discussed the errors caused by use of a constant dispersion coefficient. Other investigations followed (see, for example, Galeati *et al.* [1992] and Xue *et al.* [1995] for reviews).

These studies focused on large-scale (kilometers) saltwater intrusions in aquifers and hence did not provide information on the hydraulics and salinity distributions in the vicinity of the shore (say, meters). The beach surface was assumed to be vertical, while in reality it commonly has a mild slope. In addition, tidal fluctuations and water flow in the unsaturated zone were neglected. This large-scale approach is designated henceforth as the "aquifer" approach.

The effect of tide on beach hydraulics has been investigated by many researchers [Philip, 1973; Nielsen, 1990; Boufadel *et al.*, 1998]. Philip [1973] considered a rectangular beach and proved analytically that the average water table in the beach is above the average sea water level. Nielsen [1990] expanded the work by Philip [1973] to include sloping beaches and also found that the beach water table should be above the average sea level. Both of these researchers used the Dupuit [Bear, 1972] approach in formulating the groundwater flow problem. The Dupuit approach does not account for water flow in the unsaturated zone and treats the water flow below the water table as horizontal (i.e., neglects the vertical component of the water velocity). Boufadel *et al.* [1998] presented experimental data and modeling results for the rise and fall of the laboratory beach (Figure 1) water table due to tide, which showed a tide-averaged seaward hydraulic gradient.

Wise *et al.* [1994] numerically modeled the salinity distribution of an Alaskan beach that was subjected to tide and had fresh groundwater inflow. They used the Dupuit approach and assumed that the transient salinity distribution in the beach due to tide can be simulated as a series of steady state salinity distributions; at each discrete tidal level (corresponding to the beginning of a time step) they found the location of the water table by the Dupuit approximation and solved for the salinity distribution using Glover's [1959] analytical solution, and then they proceeded to the next time step. According to the numerical results of Wise *et al.* [1994] the fresh water floats above the saltwater wedge throughout the tidal cycle. On the basis of their analysis, Wise *et al.* [1994] proposed to apply dissolved nutrients in a trench landward of the beach, relying on the freshwater flow to carry the nutrients to the bioremediation zone.

Although the aquifer and Dupuit approaches allow the de-

velopment of analytical and/or relatively simple numerical solutions for the hydraulics in the saturated zone, they do not provide any information on the salinity distribution above the water table. This work shows that even in the saturated zone, these approaches are not appropriate for sloping beaches subjected to tides, where the flow is highly two dimensional.

### 3. MARUN Model

The marine unsaturated (MARUN) model [Boufadel *et al.*, 1999a] is a two-dimensional finite element model that can simulate water flow and solute transport in variably saturated media, taking into account the effect of the solute concentration on water density and viscosity. The dependence of water density  $\rho$  ( $ML^{-3}$ ) on the salt concentration in the MARUN model is obtained by fitting a regression curve for the density versus salt concentration:

$$\frac{\rho}{\rho_o} = (1.0 + \varepsilon c) = \beta, \quad (1)$$

where  $\rho_o = 0.9982 \text{ kg L}^{-1}$  is the freshwater density,  $c$  is the salt concentration expressed in grams of salt per liter of solution, and  $\varepsilon$  is a fitting parameter expressed in  $L \text{ g}^{-1}$ . Similarly, the dynamic viscosity  $\mu$  ( $ML^{-1}T^{-1}$ ) is related to the salt concentration by the empirical relation

$$\frac{\mu_o}{\mu} = (1.0 - \xi c) = \delta, \quad (2)$$

where  $\mu_o = 0.001 \text{ kg m}^{-1} \text{ s}^{-1}$  is the freshwater dynamic viscosity and  $\xi$  is a fitting parameter expressed in  $L \text{ g}^{-1}$ . Equations (1) and (2) are known as the state equations. Implicit in these equations and in the MARUN model is the assumption that the water temperature is constant.

In the absence of source/sink terms the equation for the conservation of the fluid mass (water plus salt) can be written as [Boufadel *et al.*, 1999a]

$$\begin{aligned} \beta \phi \frac{\partial S}{\partial t} + \beta S_o S \frac{\partial \psi}{\partial t} + \phi S \frac{\partial \beta}{\partial t} &= \frac{\partial \left( \beta \delta K_x \frac{\partial \psi}{\partial x} \right)}{\partial x} \\ &+ \frac{\partial \left( \beta \delta K_z \frac{\partial \psi}{\partial z} \right)}{\partial z} + \frac{\partial (\beta^2 \delta K_z)}{\partial z}, \end{aligned} \quad (3)$$

where  $t$ ,  $x$ , and  $z$  represent the time, the horizontal coordinate, and the vertical coordinate, respectively. The term  $\phi$  (dimensionless) is the porosity,  $S$  (dimensionless) is the soil moisture ratio (soil moisture divided by  $\phi$ ),  $S_o$  ( $L^{-1}$ ) is the specific storage per unit fluid weight,  $\psi$  ( $L$ ) is the pressure head, and  $K_x$  ( $LT^{-1}$ ) and  $K_z$  ( $LT^{-1}$ ) are the horizontal and vertical freshwater hydraulic conductivities, and they are assumed parallel to the major axes of anisotropy. The left-hand side of (3) represents the variation of water mass with time due to variation of soil moisture (the first term), matrix compaction/expansion (the second term), and variation of salt concentration. The right-hand side of (3) represents the variation of water mass in space due to the variation in space of the horizontal flow (the first term) and the vertical flow (the second and third terms).

The soil moisture and the freshwater hydraulic conductivity are related by the *van Genuchten* [1980] model:

$$S = 1, K_x = K_{x_o}, K_z = K_{z_o} \quad \psi \geq 0.0, \quad (4a)$$

where  $K_{x_o}$  and  $K_{z_o}$  are the saturated horizontal and vertical freshwater hydraulic conductivities, respectively.

For  $\psi < 0.0$  the effective saturation ratio  $S_e$  is given by

$$S_e = \frac{S - S_r}{1 - S_r} = \left[ \frac{1}{1 + (\alpha|\psi|)^n} \right]^m, \quad (4b)$$

and  $K_x$  and  $K_z$  are given by

$$K_j = K_{j_o} S_e^{(1/2)} [1 - (1 - S_e^{1/m})^2], \quad (4c)$$

where  $j = (x, z)$ ,  $m = 1 - (1/n)$ ,  $S_r$  is the residual saturation ratio, and  $|\psi|$  is the absolute value of  $\psi$ . The parameter  $\alpha$  ( $L^{-1}$ ) represents a characteristic pore size, and higher  $\alpha$  values imply a coarser material. The inverse of  $\alpha$  provides an estimate of the capillary fringe (zone of considerable moisture). The term  $n$  (dimensionless) represents the uniformity of the pores, and higher values of  $n$  imply a more uniform pore size distribution [van Genuchten, 1980]. Note that the relative hydraulic conductivity  $K = K_j/K_{j_o}$  ( $j = x, z$ ) is the same in both the  $x$  and the  $z$  directions. Implicit in (4a)–(4c) is the assumption that the salt concentration does not affect the capillary-retention relation, an assumption adopted by *Forkel and Celia* [1992].

In the absence of source/sink terms the salt transport equation may be written as [Boufadel *et al.*, 1999a]

$$\phi S \frac{\partial c}{\partial t} = \beta \nabla \cdot (\phi S D \cdot \nabla c) - \mathbf{q} \cdot \nabla c, \quad (5)$$

where  $\mathbf{q}$  is the Darcy flux vector given by

$$q_x = -K_x \delta \left( \frac{\partial \psi}{\partial x} \right), \quad (6a)$$

$$q_z = -K_z \delta \left( \frac{\partial \psi}{\partial z} + \beta \right). \quad (6b)$$

Notice that  $\delta$  is less than 1.0 for  $c > 0$ , indicating that a higher resistance to water flow is encountered for salt water in comparison to fresh water. The term  $D$  in (5) represents the physical dispersion tensor given by

$$\phi S D_{xx} = a_L \frac{(q_x)^2}{\|q\|} + a_T \frac{(q_z)^2}{\|q\|} + \phi S \tau D_f, \quad (7a)$$

$$\phi S D_{zz} = a_T \frac{(q_x)^2}{\|q\|} + a_L \frac{(q_z)^2}{\|q\|} + \phi S \tau D_f, \quad (7b)$$

$$\phi S D_{xz} = \phi S D_{zx} = (a_L - a_T) \frac{q_x q_z}{\|q\|}, \quad (7c)$$

where  $a_L(L)$  and  $a_T(L)$  are the longitudinal and transverse dispersivities, respectively,  $D_f(L^2 T^{-1})$  is the diffusion coefficient, and  $\tau$  (dimensionless) is the domain tortuosity. The first two terms on the right-hand side of (7a) and (7b) represent salt transport by mechanical dispersion while the third term represents salt transport by molecular diffusion. Equation (7c) accounts for the situations where the direction of the local velocity does not coincide with the major axes  $x$  and  $z$  [Bear, 1972].

In the MARUN model the water flow and salt transport equations are discretized in space by the Galerkin finite element method [Pinder and Gray, 1977] using linear triangular elements and integrated in time using backward Euler with

mass lumping [Celia *et al.*, 1990]. Nonlinearity in the water flow equation is accounted for by solving the equation iteratively using the modified Picard method [Celia *et al.*, 1990].

When high salt variations (say,  $>10 \text{ g L}^{-1}$ ) are being simulated in the MARUN model, the water flow and the salt transport equations are coupled. The primary coupling arises in the equations through the hydraulic conductivity (due to viscosity variation) and the body force term (due to density variation) of the fluid flow equation and the advection terms of the solute transport equation. A second coupling enters the equations through the velocity-dependent hydrodynamic dispersion. Therefore these equations are solved iteratively at each time step until no change in the solution is observed (within a preset tolerance). More information on the implementation of the MARUN model is given by Boufadel *et al.* [1998, 1999a, 1999b].

When small salt variations that do not affect the water density are being simulated in the MARUN model, the water flow equation does not depend on the salt concentration and is therefore solved separately from the salt transport equation.

Results from the MARUN model in application to the laboratory beach are presented in section 6.

## 4. Experimental Methodology

### 4.1. Experimental Layout

The facility used in the experiment consisted of an 8 m long  $\times$  2 m high  $\times$  0.6 m wide carbon steel tank as shown in Figure 1. The tank was placed on eight adjustable supports (0.1  $\times$  0.1 area and 0.1 height). Hence the bottom of the tank was  $\sim$ 0.1 m above the concrete floor. This was done to allow air circulation around the tank to minimize thermally generated buoyancy currents. One of the long vertical sides was made transparent by replacing the steel sheets with plexiglass.

The sand in the tank was graded at a slope of 10% from a height of 115 to 65 cm and at 50% slope from 65 cm to zero, which results in a total horizontal sand coverage at the bottom of the tank of  $\sim$ 630 cm (Figure 1). The sand was held in place at 30 cm from the left wall (Figure 1) by a screen made of expanded steel and a fine mesh. The pores of the screen were large enough (0.1 mm) to allow unhindered passage of water through them.

The tide was simulated by pumping water in and out of the tank via two vertical manifolds placed on the opposite long vertical sides of the tank (Figure 1). To simulate “regional” water table and concentration landward of the beach, water was pumped in the tank through a 30 cm long manifold placed across the bottom of the tank, 15 cm to the left of the screen (i.e., the manifold is a perforated tube placed perpendicular to the plan of Figure 1 at the location ( $x = -15 \text{ cm}$ ,  $z = 0.0 \text{ cm}$ ), which coincides with the location of pressure transducer 1 (PT1)). A mixer was placed in the open water at the sea side to achieve a uniform salt concentration at the sea side. Two sacrificial zinc plates were placed in the tank on both ends to reduce corrosion of the steel tank.

### 4.2. Sand Properties

The sand used was an artificial sand composed mostly of silica ( $\text{SiO}_2$ ) from Sidley, Inc., Cleveland, Ohio. It had a median size of 1.0 mm and a very narrow particle size distribution, varying between 0.8 and 1.2 mm. The shape of particles was classified as “round to semiangular.” These sand properties resulted in very little sand transport by suspension. The sand

porosity was determined to be 0.38, by filling a 4 L beaker with well-drained sand and adding a sufficient amount of water to produce ponding conditions at the sand surface. The ratio of the volume of the added water to the apparent volume of the sand is, by definition, the porosity of the medium. The porosity of the sand in the tank was estimated in situ by observing the settlement of the beach sand profile that occurred a few days after the sand was placed in the tank and covered with water. The reduction in sand height in the beach was  $\sim$ 4%, resulting in a porosity of  $(1-0.04)(0.38) = 0.365$ . A value of 0.36 was adopted to be used in the model.

Capillary-retention experiments [Bear, 1972] (some reported by Boufadel [1998]) gave the following values:  $\alpha = 0.18 \text{ cm}^{-1}$ ,  $n = 2.9$ ,  $S_r = 0.01$ . The saturated hydraulic conductivity of the sand was estimated using Hazen’s formula to be  $\sim$ 0.3  $\text{cm s}^{-1}$ , and a falling head test measurement gave a value of  $\sim$ 1.0  $\text{cm s}^{-1}$  [Cedergren, 1967]. These measured values of  $\alpha$ ,  $n$ ,  $S_r$ , and the saturated hydraulic conductivity were considered as prior estimates and were “improved” by fitting the model to the experiments reported in section 6.

### 4.3. Water Solution Properties

A commercial grade of sodium chloride (NaCl) salt (Morton System Saver, Morton, Chicago, Illinois) was used in the experiments. The composition of the commercial salt was not known exactly, but it was suspected to contain impurities that have different hydration properties from pure NaCl. Measurements of water density at various concentrations of the commercial salt were taken, and a fit of (1) to the data gave  $\varepsilon = 7.44 \times 10^{-4} \text{ L g}^{-1}$  (the plot is shown by Boufadel [1998, p. 243]). The value of  $\varepsilon$  for pure NaCl solution is  $6.46 \times 10^{-4} \text{ L g}^{-1}$  [Boufadel *et al.*, 1999a]. Because of the absence of viscosity data for the commercial salt solution the parameter  $\delta$  (equation (2)) was determined by fitting a straight line to concentration and viscosity data of pure NaCl obtained from Weast [1983, p. D261]. A value of  $\delta = 1.566 \times 10^{-4} \text{ L g}^{-1}$  was adopted. We observed in this work that viscosity effects are small in comparison to density effects for the concentration range considered ( $<32 \text{ g L}^{-1}$ ). The effect of error in the estimation of  $\delta$  is discussed in section 6.3.

### 4.4. Measuring Devices

The experiments required the measurements of the positive pressure at the bottom of the tank and the salt concentration. The positive water pressure at the bottom was measured using pressure transducers (PT, model 1151AP, Fisher Scientific, Hampton, New Hampshire) that have a reading accuracy of  $\sim$ 2.0 mm of water. The PTs were placed 3.0 cm above the bottom of the tank (Table 1 and Figure 1) and were logged by the Strawberry Tree data software (Strawberry Software Inc., Sunnyvale, California). This software was used also to control the inflow and outflow pumps, which regulated the water flow and level in the tank.

The salt concentration was measured by conductivity meters (CM, CDCN 108, Omega Engineering, Stamford, Connecticut) that measure the electrical conductivity of the water solution, which varies with the salt concentration. The CMs were in the shape of a hollow disk (doughnut) which had the dimensions 10 cm (external diameter), 2.5 cm (internal diameter), and 3 cm (thickness). Early experimentation with the CMs showed that they are not reliable when in direct contact with sand. For this reason, the CMs were suspended in special plexiglass casings to separate them from the sand while allow-

ing their contact with the solution. The casings were hollow cubes with a side length of 15 cm; they were slotted on all sides and covered with a 0.1 mm stainless steel screen. The CMs were calibrated in situ simultaneously between an “air” value (the CMs were dry and in contact with air on all sides) and a desired maximum salt concentration in solution. The air value was obtained by draining the tank completely (in fact, a residual amount  $\sim 3$  cm high remained at the bottom). The maximum value was obtained by circulating a saltwater solution in the tank until reaching a uniform concentration. The concentration of the solution is then measured using a salinity meter and assigned to all the CMs. In situ measurement of the concentration was done because the residual water altered the salinity of the prepared suspension. Experimentation with the CMs showed that their accuracy is  $\sim 5\%$  of the measured salt concentration. For this reason, they were calibrated prior to every experiment.

The locations of the CMs’ centers are given in Table 1, and their positions along the length of the tank are shown in Figure 1. The horizontal distances of the CMs from the plexiglass wall were different to ensure that a sensor does not greatly alter the flow lines to another sensor along the general flow direction. The data from all sensors were logged at an interval of 30 s.

## 5. Experimental and Numerical Approach

The goal is to investigate the effects of tide and buoyancy (due to the presence of fresh water) on beach hydraulics and hydrodynamics. This was achieved in two experiments: The experiment of case 1 was designed to investigate the effects of tide only, while the experiment of case 2 was designed to investigate the combined effects of tide and buoyancy. The maximum change of the solute (salt) concentration was  $\sim 2.4$  g  $L^{-1}$  for case 1 and 32 g  $L^{-1}$  for case 2. Thus the salt in case 1 acts as a tracer. The salinity variation of case 2 was chosen to represent typical salinity variation on beaches at the coasts of the continental United States containing a freshwater lens. The hydraulic and hydrodynamic parameters of the laboratory beach were estimated by fitting the MARUN model to pressure head and concentration data from both experiments.

### 5.1. Experiment

Prior to each of the experiments the tank was filled with fresh water (tap water), and a steady state pressure distribution was established where the pressures at PT1 and PT5 were 85 and 70 cm, respectively. This was done by pumping water in the tank to the left of the screen and pumping water out of the tank at the sea side. Then, the inflow solution was changed to salt water and was circulated through the tank until a uniform salt concentration was reached. The uniform concentration was 2.6 g  $L^{-1}$  for case 1 and 32 g  $L^{-1}$  for case 2.

Each experiment started by reintroducing fresh water (tap water) to the left of the screen through the same manifold used to introduce salt water, and this was done under the same steady state hydraulic regime. Because of the difference in water head between PT1 and PT5 the fresh water propagated in the beach toward the sea side causing a reduction of the salinity in the beach. The tidal cycle was started when the concentration at CM9 reached  $\frac{1}{3}$  of its initial value. The tidal level was controlled by the reading at PT5, which was set to vary between 70 and 95 cm. The intertidal zone covered the beach surface from  $x = 200$  cm to  $x = 450$  cm, where the slope is 10%. The tidal period was  $\sim 22$  min.

**Table 1.** Locations of Pressure and Concentration Sensors<sup>a</sup>

| Sensor            | $x$ , cm | $z$ , cm | $y$ , cm |
|-------------------|----------|----------|----------|
| PT1               | -15      | 3        | 60       |
| PT2               | 78       | 3        | 60       |
| PT3               | 147      | 3        | 60       |
| PT4               | 232.5    | 3        | 60       |
| PT5               | 364      | 3        | 60       |
| PT6               | 645      | 3        | 60       |
| CM1               | 70       | 30       | 20       |
| CM2               | 70       | 80       | 40       |
| CM3               | 150      | 40       | 20       |
| CM4               | 150      | 70       | 40       |
| CM5               | 150      | 80       | 25       |
| CM6               | 200      | 60       | 30       |
| CM7               | 275      | 20       | 40       |
| CM8               | 275      | 50       | 20       |
| CM9               | 275      | 71       | 25       |
| CM10              | 400      | 20       | 20       |
| CM11              | 400      | 60       | 40       |
| CM12              | 500      | 50       | 30       |
| CM13 <sup>b</sup> | 550      | 60       | 30       |
| CM14 <sup>b</sup> | -15      | 40       | 30       |

<sup>a</sup>Here,  $x$  is the horizontal distance from the screen (positive seaward),  $z$  is the elevation from the bottom of the tank, and  $y$  is the horizontal distance from the plexiglass wall (positive inward perpendicular to the plane of Figure 1).

<sup>b</sup>The sensor is in open water (Figure 1).

The control of the water pressure at PT1 was designed to simulate a water table landward of a natural beach whose height (the water table) is dictated both by tidal forcing and by the regional groundwater table. Studies have shown that the effect of tide is greatest near a high tide, where the water table landward of the beach responds rapidly to the tidal level [Philip, 1973; Nielsen, 1990; Boufadel et al., 1998]. In contrast, the water table landward of the beach lags behind a falling tide and is more affected by the regional groundwater table, especially near a low tide. In many cases, “hydraulic separation” occurs between the water table in the beach and the water level at sea whereby a seepage face develops at the beach surface (see, for example, the experimental results of Nielsen [1990]). The presence of a regional groundwater table was accounted for in the present experiments by controlling the minimum water pressure at PT1 (which occurs near a low tide), by pumping fresh water through the manifold to the left of the screen whenever the water pressure at PT1 dropped below 85 cm. The tolerance for cessation and initiation of pumping was plus and minus 0.2 cm of water from the 85 cm pressure head at PT1, respectively.

The salinity of the tap water varied between 0.15 and 0.2 g  $L^{-1}$  during the course of the experiments; hence an average value of 0.175 g  $L^{-1}$  was adopted. The fact that the salinity of the “fresh water” was not equal to zero does not affect the significance of the results because the effects of buoyancy result from concentration gradients and do not depend on the actual value of concentration.

The injected fresh water contained air bubbles, which increased the mixing in the open water behind the screen. Salinity measurements at different heights to the left of the screen indicated that the open water there was well mixed.

Prior to the tidal action a seepage face of length  $\sim 5$  cm was observed at the beach surface. The length of the seepage face varied during the tidal cycle. It disappeared for  $PT5 \geq 85$  cm and reached  $\sim 20$  cm at low tide.

**Table 2.** Hydraulic and Hydrodynamic Parameters of the Laboratory Beach

| Parameter           | Value                          | Units                       |
|---------------------|--------------------------------|-----------------------------|
| $K_{x_o} = K_{z_o}$ | 0.65 (case 1)<br>0.75 (case 2) | $\text{cm s}^{-1}$          |
| $\alpha$            | 0.125                          | $\text{cm}^{-1}$            |
| $n$                 | 3.50                           | dimensionless               |
| $S_p$               | 0.01                           | dimensionless               |
| $S_o$               | 0.0                            | $\text{cm}^{-1}$            |
| $a_L$               | 0.75                           | cm                          |
| $a_T$               | 0.25                           | cm                          |
| $\tau D_f$          | $10^{-6}$                      | $\text{cm}^2 \text{s}^{-1}$ |
| CONVP               | 0.1                            | cm                          |

## 5.2. Modeling

The beach domain was discretized in space using two meshes. The coarse mesh contained 4788 nodes and 9240 triangular elements; the average spacing between nodes varied from 3.5 to 1.5 cm, being largest at ( $x = 0, z = 0$ ) and smallest at ( $x = 500 \text{ cm}, z = 65 \text{ cm}$ ). The fine mesh contained 16,240 nodes and 31,806 triangular elements; the spacing between nodes varied from  $\sim 2.2 \text{ cm}$  at ( $x = 0.0, z = 0.0$ ) to  $\sim 0.5 \text{ cm}$  at ( $x = 500 \text{ cm}, z = 65 \text{ cm}$ ). For both meshes the time step for the numerical simulation was set equal to 30 s.

The flow equation was solved independently of the transport equation for case 1 because the numerical results obtained by this approach were essentially the same as those obtained by coupling the two equations (hence the salt acts as tracer). For case 2 the flow equation was coupled to the transport equation by one iteration (i.e., updating). The convergence criterion for pressure in the Picard iterative scheme was CONVP = 0.1 cm (Table 2). The boundary and initial conditions are given in sections 5.2.1 and 5.2.2.

**5.2.1. Boundary conditions.** For the Flow equation at the screen ( $x = 0$ ) a Dirichlet boundary condition below the water level (in the open water left of the screen) is

$$\psi(0, z) = H(\text{PT1}) - z[1 + \varepsilon c(\text{CM14})],$$

where  $H(\text{PT1})$  is the head at PT1,  $c(\text{CM14})$  is the concentration of CM14, and  $\varepsilon$  is from (1). This represents a hydrostatic pressure distribution for  $\psi(0, z) \geq 0$ . For  $\psi(0, z) < 0$  a Neuman boundary condition was assigned:  $\delta\psi/\delta x = 0$ .

For the flow equation at the beach surface,

$$\psi(x, z) = H(\text{PT5}) - z[1 + \varepsilon c(\text{CM13})] \quad \psi(x, z) \geq 0$$

(Dirichlet). For  $\psi(x, z) < 0$  a seepage face boundary condition was applied. Implementation of the seepage face boundary condition was done according to the method of Neuman [1973] and is discussed in detail by Boufadel *et al.* [1998, 1999c].

For the transport equation at both  $x = 0$  and at the beach surface, for  $\psi(x, z) < 0$ ,  $\delta c/\delta x = 0$  (Neuman). For  $\psi(x, z) \geq 0$  a check for the water velocity was set: If the water is entering the beach, then a Dirichlet boundary condition was assigned with  $c(0, z) = c(\text{CM14})$  at  $x = 0$  and  $c(x, z) = c(\text{CM13})$  at the beach surface. If water is leaving the beach, then a Neuman boundary condition was assigned,  $\delta c/\delta x = 0$ , which represents the so-called outflowing boundary condition, where water leaves the porous domain without a change in concentration. This boundary condition is discussed further by Galeati *et al.* [1992] and Boufadel *et al.* [1999a].

**5.2.2. Initial conditions.** The initial pressure head and concentration distributions were obtained by running the MA-RUN model until reaching a steady state with the pressure heads at PT1 and PT5 set equal to 85 and 70 cm, respectively, and with a Dirichlet boundary to the left of the screen ( $c = 2.6 \text{ g L}^{-1}$  for case 1 and  $c = 32 \text{ g L}^{-1}$  for case 2). The initial concentration to be used in the experiments was thus  $c(x, z, t = 0) = 2.6 \text{ g L}^{-1}$  for case 1 and  $c(x, z, t = 0) = 32 \text{ g L}^{-1}$  for case 2.

## 6. Results

The hydraulic and hydrodynamic parameters used to simulate the experiments are listed in Table 2. A discussion on these parameters is provided later in section 7. The readings of CM2 and CM5 are not reported because these sensors failed during the experiments.

### 6.1. Case 1

Modeling results obtained from the fine grid were essentially the same as those obtained from the coarse grid. Hence grid convergence has been achieved in the coarse grid. Figure 2 shows the experimental and modeling results of case 1; the overall agreement between them is good. We now focus on the experimental results.

The fluctuation of the reading of CM13 (Figure 2e) with time was due to the fact that the mixing in the open water at sea was set at a moderate level in order not to affect the hydraulics within the sand. Because of the proximity of CM13 to the beach surface, low-salinity plumes leaving the beach tended to pass through it, resulting in the sharp decreases in Figure 2e.

For  $t < 2.1$  hours (the time at which the tidal cycle was started, see Figure 2h) the concentrations at all sensors decreased with time. However, different behavior of the concentration was observed for  $t > 2.1$  hours depending on the location of the sensor. Sensors located in the intertidal range ( $200 \text{ cm} < x < 450 \text{ cm}$ ) near the beach surface tended to increase with time; a good illustration is provided in Figure 2d, which shows the concentration at sensors CM7, CM8, and CM9 located in the same vertical plane. One notes in Figure 2d that while the concentration at CM7 kept decreasing with time, the concentration at CM8 increased for  $t > 2.1$  hours, but remained lower than the concentration at CM9. Similarly, the concentration at CM11 (Figure 2f) increased with time for  $t > 4.0$  hours, while Figure 2e shows that the concentration at CM10, which is in same vertical plane of CM11 (see Figure 1), was continually decreasing with time. This indicates that tidal action resulted in an inverted salinity distribution in the beach, with salt water overtopping the fresh water. Figures 2d and 2e show that for  $t > 4$  hours a periodic steady state salinity distribution was reached in the intertidal range of the beach ( $200 < x < 450 \text{ cm}$ ) and persisted for more than 10 tidal cycles (until the end of the experiment,  $t = 9$  hours).

The model simulated well the general behavior of observed concentrations (Figures 2a–2f) and water pressure (Figures 2g and 2h) both before and after the tidal cycle started. The parameter values used in the simulation are given in Table 2. A discussion of the fit is provided at the end of this section.

Figure 3 shows modeled salinity, pressure, and Darcy fluxes at times  $t = 2.10, t = 2.325, t = 8.60,$  and  $t = 8.733$  hours. These times were selected to occur just before the tidal cycle, at the first high tide, at the last low tide, and at the last high tide.

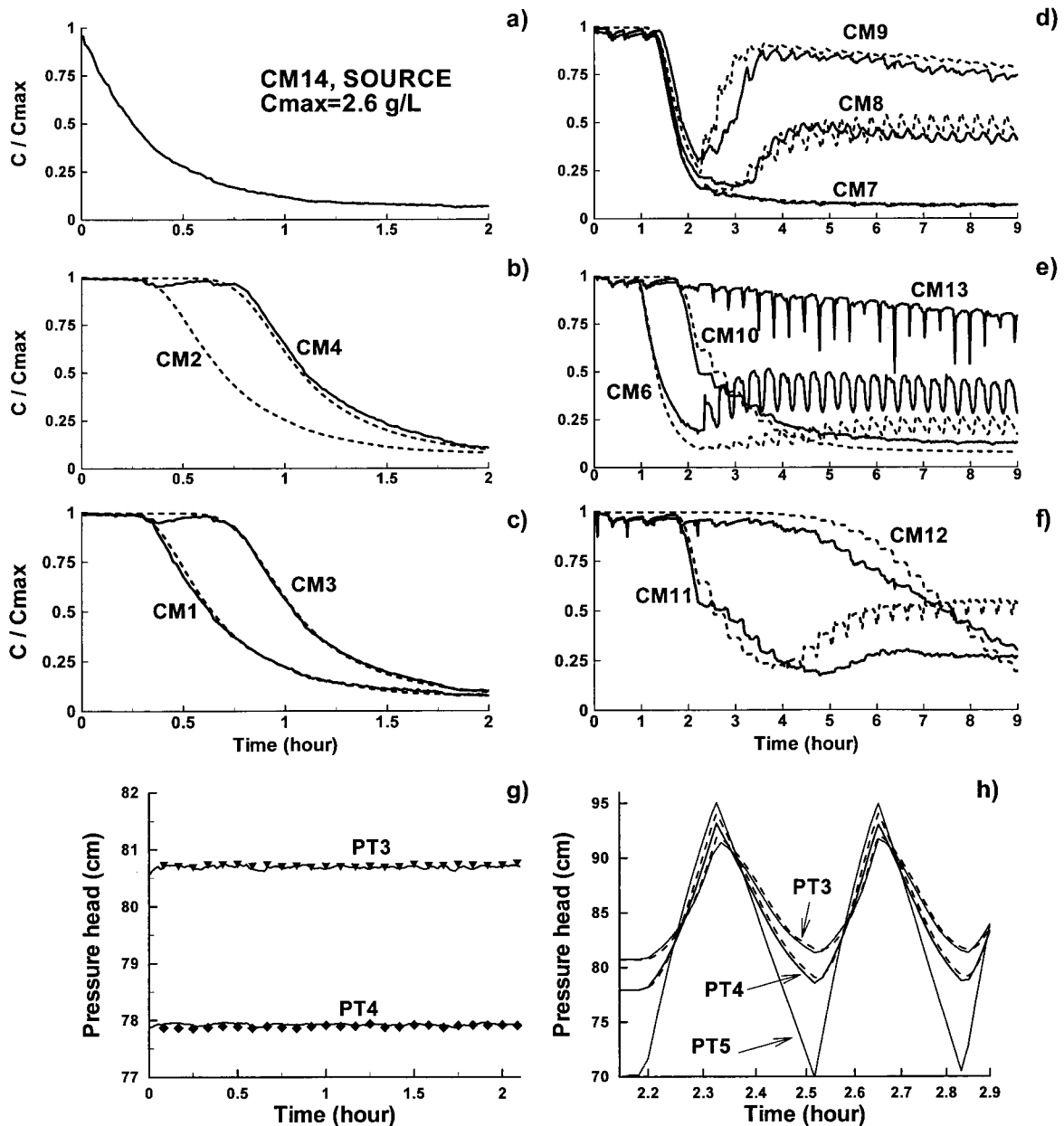


**Figure 2.** Observed and simulated concentrations (Figures 2a–2f) and pressure heads (Figures 2g and 2h) of case 1 (the effect of salt on water properties is negligible).

At  $t = 2.1$  hours, Figure 3 shows that water leaves the beach in the upward direction, perpendicularly to the beach surface. This should be expected because the submerged beach surface is an equipotential, and velocity vectors are perpendicular to it. The maximum water velocity occurred at the intersection of the water table and beach surface. This is due to the fact that a constant head (pressure head plus elevation head) was assumed at sea; hence a water mass going seaward to leave the beach proceeds in the direction of minimum head loss (or shortest path), which in this case is upward toward the intersection of the water table and the beach surface. Seaward horizontal motion results in higher head loss due to friction with the sand particles. It is for this reason that the concentration at CM13 placed at  $z = 60$  cm was decreased sharply when water was leaving the beach (i.e., near a low tide), while CM12 (which is within the beach, seaward of the intersection

location of the water table and the beach surface) was still at its high initial value. In other words, most of the fresh water left the beach landward of CM12. Note that because the unsaturated beach surface is not an equipotential (it is a no-flow boundary), the Darcy flux is not perpendicular to the beach surface at the intersection of the water table and the beach surface.

With  $\alpha = 0.125 \text{ cm}^{-1}$  (Table 2) the capillary fringe of this sand is estimated as  $1/0.125 = 8$  cm. Figure 4,  $t = 2.10$  hours, shows that the fresh water crossed the water table and propagated in the capillary fringe but not much above it. The reader is referred to the work of Boufadel *et al.* [1999c] for a thorough investigation on the contribution of capillary flow to steady seepage in rectangular and trapezoidal domains.

At  $t = 2.325$  hours (the first high tide), Figure 3 shows that the rising waters at sea enter the beach perpendicular to the

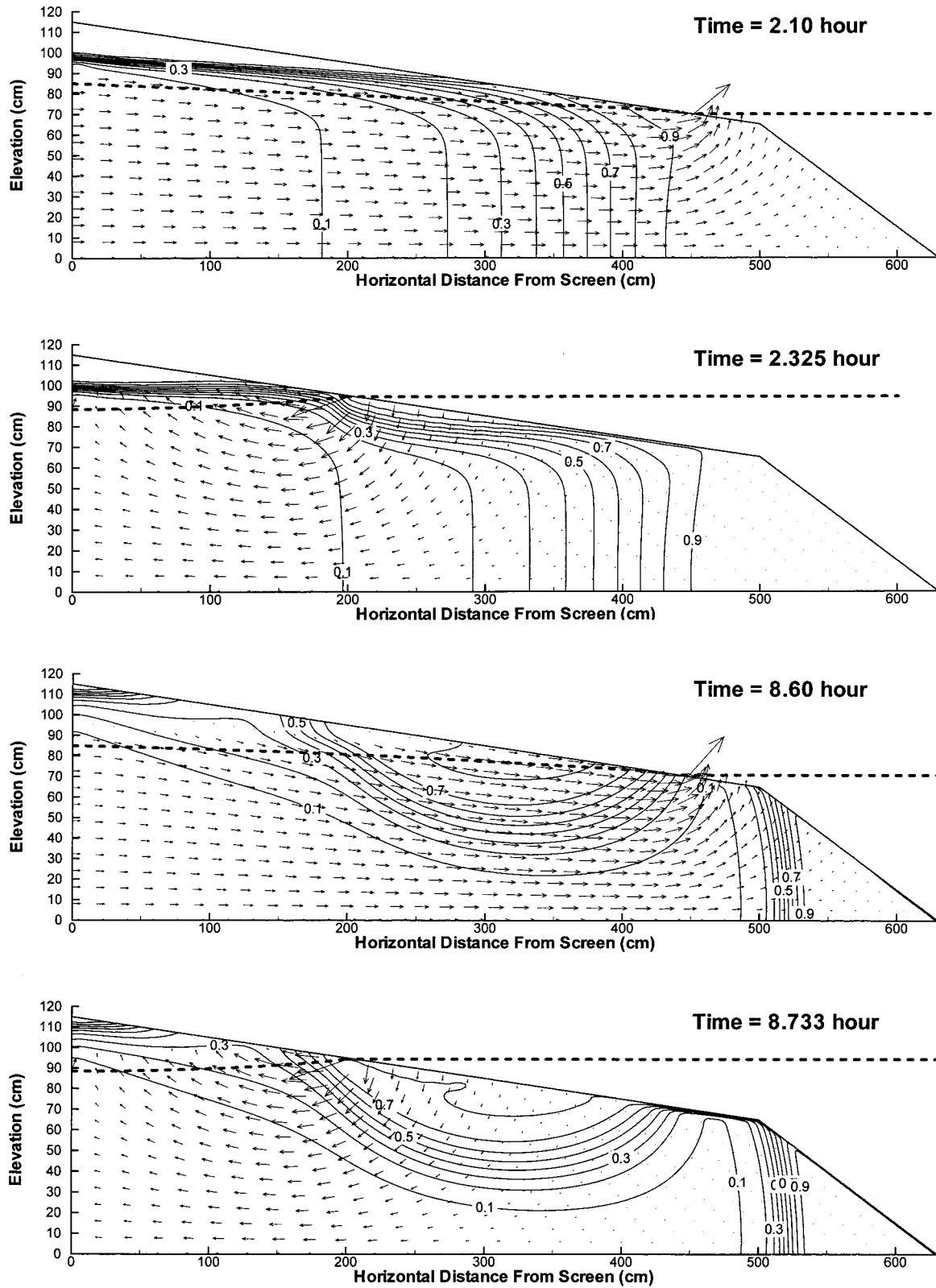


**Figure 3.** Salinity and Darcy flux distribution at four different times for case 1 (solute does not affect water properties) obtained from the fine grid. The arrows represent the Darcy flux. The dashed lines represent the water table in the beach and the water level at sea.

beach surface. It is this mechanism that produced the inverted salinity distribution in the beach. When going from  $t = 2.10$  hours to  $t = 2.325$  hours, the saltwater plume at the top section of the beach moved landward, but the saltwater plume at the low section of the beach ( $z < 60$  cm) moved seaward. The latter movement was due to fresh water propagating seaward (note, for example, the 0.3 isochlor). This demonstrates that the sloping beach surface generates a highly two dimensional flow, with a counterclockwise circulation cell occurring within the beach. Hence the Dupuit assumption, which consists of neglecting the vertical flow component with respect to the horizontal flow component, is not suitable for describing solute transport in beaches (or other systems where the subsurface interfaces with the open water by a sloping surface). The coun-

terclockwise circulation cell is apparent where water enters the beach at a quasi-vertical angle ( $t = 8.733$  hours) and leaves it at a quasi-horizontal angle ( $t = 8.60$  hours). At these later times, two saltwater plumes were present in the beach, and they were “separated” by fresh water at  $x \approx 470$  cm (if one considers the 0.1 isochlor as the “edge” of the plume). The fresh water persisted beneath the saltwater plume in the intertidal zone, and this salinity distribution was repeated every tidal cycle starting from  $t$  larger than  $\sim 4$  hours ( $\sim 10$  tidal cycles). This circulation cell has major implications on nutrient transport in beaches (discussed in section 10).

Under tidal action the reading at PT5 was generally lower than the reading at PT1. The average readings (averaged over

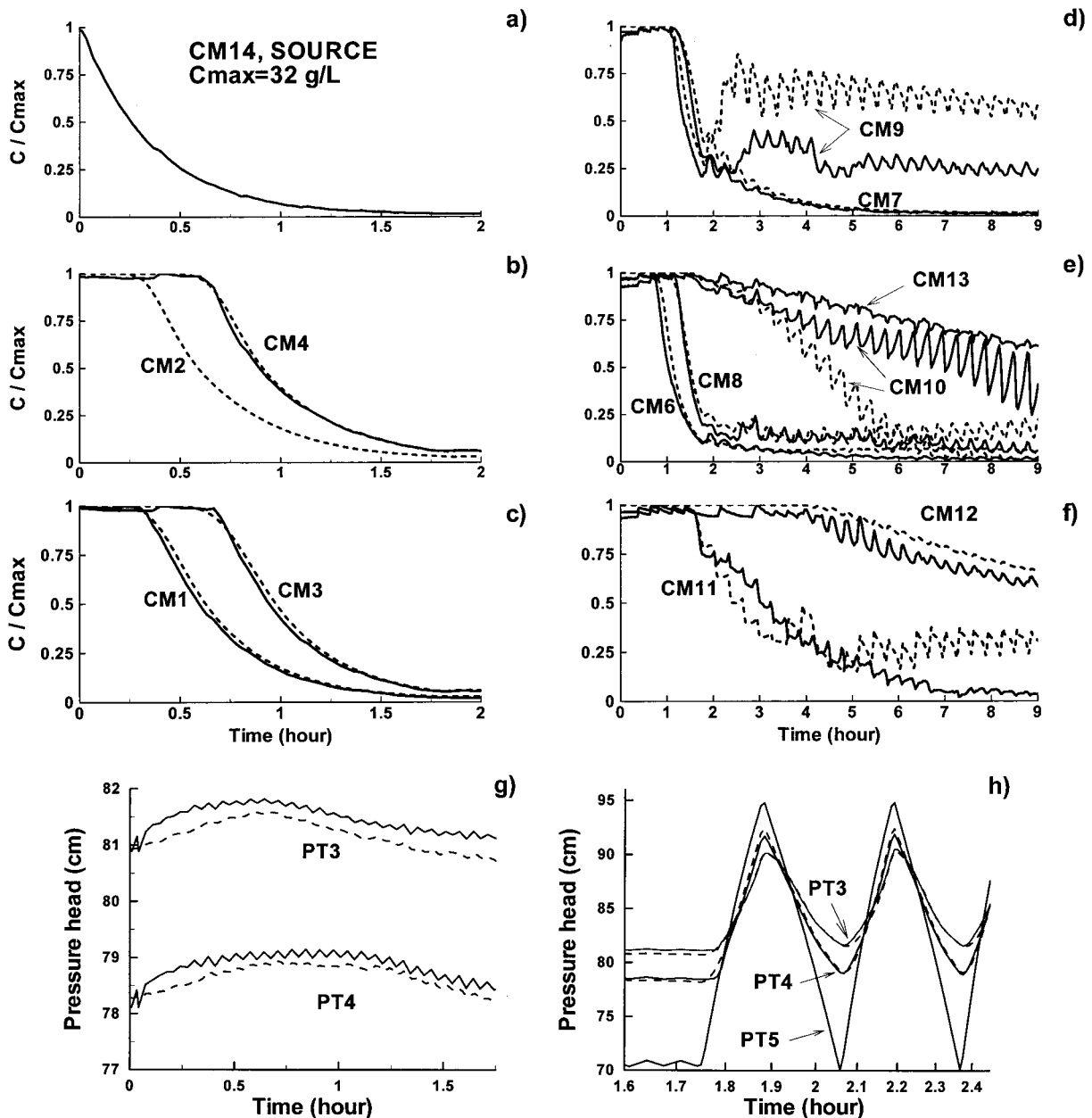


**Figure 4.** Observed and simulated concentrations (Figures 4a–4f) and pressure heads (Figures 4g and 4h) of case 2 (density-and-viscosity-dependent flow) obtained from the coarse grid.

all the tidal cycles) at PT1 and PT5 were 87 and 83 cm, respectively, which indicates that a persistent seaward hydraulic gradient existed in the beach. The presence of this gradient cannot be attributed only to control of the level at PT1. Using the same experimental setup, Boufadel *et al.* [1998] conducted experiments where PT1 was not controlled (i.e., allowed to decrease following a low tide) and found that tidal action alone causes the seaward hydraulic gradient.

## 6.2. Quality of Fit

The following factors influenced the agreement between the numerical and experimental results:

1. Although the degree of heterogeneity of the laboratory beach sand is expected to be small, the relatively small scale of the experimental setup makes concentration modeling results highly sensitive to local heterogeneity. The presence of heterogeneity can be detected by comparing, for example, CM6 and CM10 in Figure 2e. Prior to the tidal cycle ( $t < 2.10$  hours) the model predicted an earlier arrival of the front at CM6 and a late arrival at CM10. Hence one hydraulic conductivity value cannot match both CM6 and CM10, which indicates the presence of heterogeneity, and a possible three-dimensional (3-D) flow since there is no reason for heterogeneity to be restricted to a 2-D plane.

2. In modeling the experiment each CM was assumed to be located at one geometric point (given in Table 1) while in reality it occupies a certain volume and was placed in a plexiglass box (Figure 1). Hence the experimental value at a CM could be viewed as a volume-averaged value because the CM senses (or computes) the electric capacitance field in the plexiglass box.

3. Imperfections are present in the beach surface. As discussed in section 6.1, the beach surface greatly affects beach hydraulics because velocity vectors are perpendicular to the submerged beach surface (Figure 3). The beach slope was set by design to change from 10% to 50% at ( $x = 500$  cm,  $z = 65$  cm). However, because of scouring effects of water the location of the change of the slope was not well defined. This probably affected the flow in the beach because a 1.0 cm vertical error in the beach surface displaces the intersection point of the beach water table and the beach surface by 10 cm, which, in turn, affects the streamlines and the concentration distribution in the beach. Furthermore, the scouring effect of water created channels in the sand  $\sim 1$  cm deep and 0.5 m long on the beach surface parallel to the long sides of the tank. These probably acted as drains for water flow, generating therefore three-dimensional preferential flows toward them.

These factors made matching the observed concentrations a challenging task. Because of the fact that a cyclic transient regime was reached in the beach for  $t > 4$  hours, just a 5 cm difference in the location of the concentration front between the model and the experiment would give the impression that a major discrepancy took place. For example, Figure 2f shows a large deviation between the simulated and observed CM11, while in reality a perfect match occurs between the experimental result and the model if one considers a point just 5 cm below the location assigned to CM11 in Table 1. The same argument applies to CM6, where the simulated concentration undershot the observed one by  $\sim 0.2$  normalized concentration (Figure 2e), but Figure 3 ( $t = 8.60$  hours and  $t = 8.733$  hours) shows that the 0.5 isochlor at CM6 is above the 0.3 isochlor by only  $\sim 5$  cm.

Some of the “corrective” actions to improve the fit would be

as follows: (1) Drop the homogeneity assumption (and even the isotropy assumption) and assign zones of different permeability to the sand. (2) Average the model concentration values within the plexiglass box around each CM to account for the relatively high mixing in a volume containing water in comparison to a porous volume containing water. (3) Empirically change the slope around  $x = 500$  cm,  $z = 65$  cm to match the concentrations at CM10 and CM11. These actions were not pursued because they do not add to our understanding of the beach system.

## 6.3. Case 2

The experiment of this case was run similarly to that of case 1 with the exception that the initial salt concentration was  $32 \text{ g L}^{-1}$  (sea water at the coasts of the continental United States). Because the PTs were calibrated under freshwater conditions, the water levels and pressure values in case 1 were interchangeable. This interchangeability ceases when high salt concentration is present because in such a situation the salt concentration alters the water density. Because the constant head hydraulic boundary conditions were achieved by controlling PT1 and PT5, the water levels behind the screen and in the open water at the sea side in this experiment were lower than their corresponding values in case 1.

A small systematic error arises from the fact that the PTs were  $\sim 3.0$  cm above the tank bottom and that they were calibrated in fresh water. When measuring pressure under high-density salt water (the  $32 \text{ g L}^{-1}$ ), the maximum error is of  $\sim 0.08$  cm, a negligible amount.

Figures 4 and 5 show the observed and simulated concentrations and pressure heads as a function of time for the experiment of case 2, using the coarse and fine grids, respectively. Similarly to case 1, the tidal cycle was started when the observed concentration at CM9 reached  $\frac{1}{3}$  of its initial value, which occurred in this case at  $t = 1.67$  hours. For both grids the model simulated relatively accurately the concentration at sensors CM1, CM3, CM4, CM6, CM8, CM11, and CM12. The difference at CM9 and CM10 may be attributed to the factors mentioned in section 6.2. The only visible difference between the results of the coarse grid and those of the fine grid is in the water pressure prior to the tidal action (Figures 4g and 5g); the fine grid matched the observed pressure head better than the coarse grid, which is probably because of a better discretization near the beach surface.

Unlike case 1, the concentration at CM6 and CM8 did not rise under tidal action, as confirmed by both the experimental and the numerical results (Figures 4e or 5e). Although the model in case 2 predicted a larger rise of the normalized concentration at CM9 after the tidal cycle was started in comparison with the experimental results (Figures 4d or 5d), this rise is less than that given by the model in case 1 (Figure 2d).

Prior to the tidal cycle the pressure at PT3 and PT4 in case 2 (Figures 4g and 5g) exhibited strong variations that did not occur in case 1 (Figure 2g). This is due to the effect of high salt concentration. Because of the imposed pressure head of 85 cm at PT1, when fresh water was entering the open water area to the left of the screen, the water level was increasing to compensate for a decrease in the salinity. Because of the incompressibility of water each increase in the water level to the left of the screen resulted in an immediate increase in the water table throughout the beach. This occurred while the salinity in the beach (including that in the capillary fringe) was at its maximal value of  $32.0 \text{ g L}^{-1}$  so that the water pressure at the

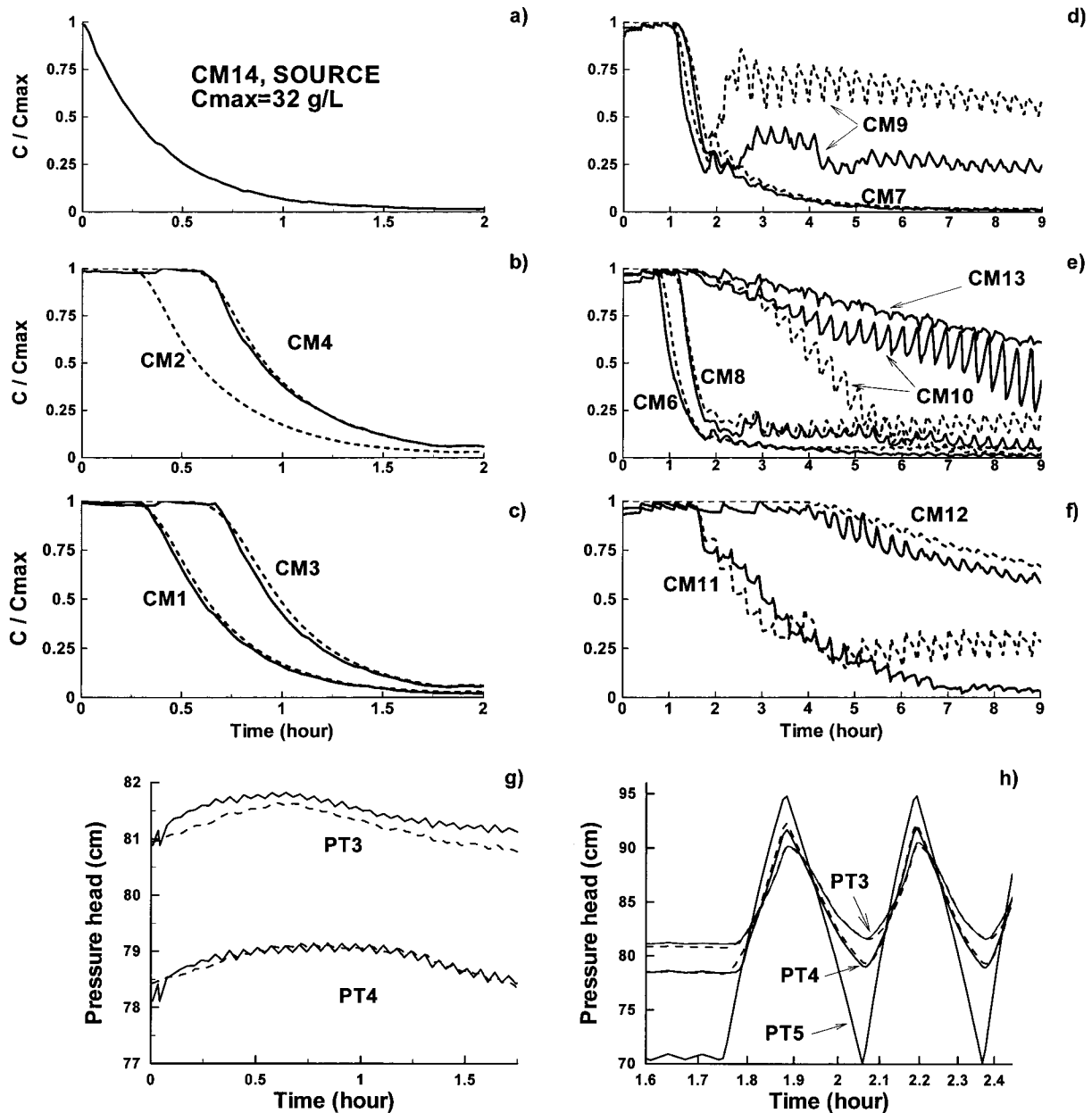


**Figure 5.** Observed and simulated concentrations (Figures 5a–5f) and pressure heads (Figures 5g and 5h) of case 2 (density-and-viscosity-dependent flow) obtained from the fine grid.

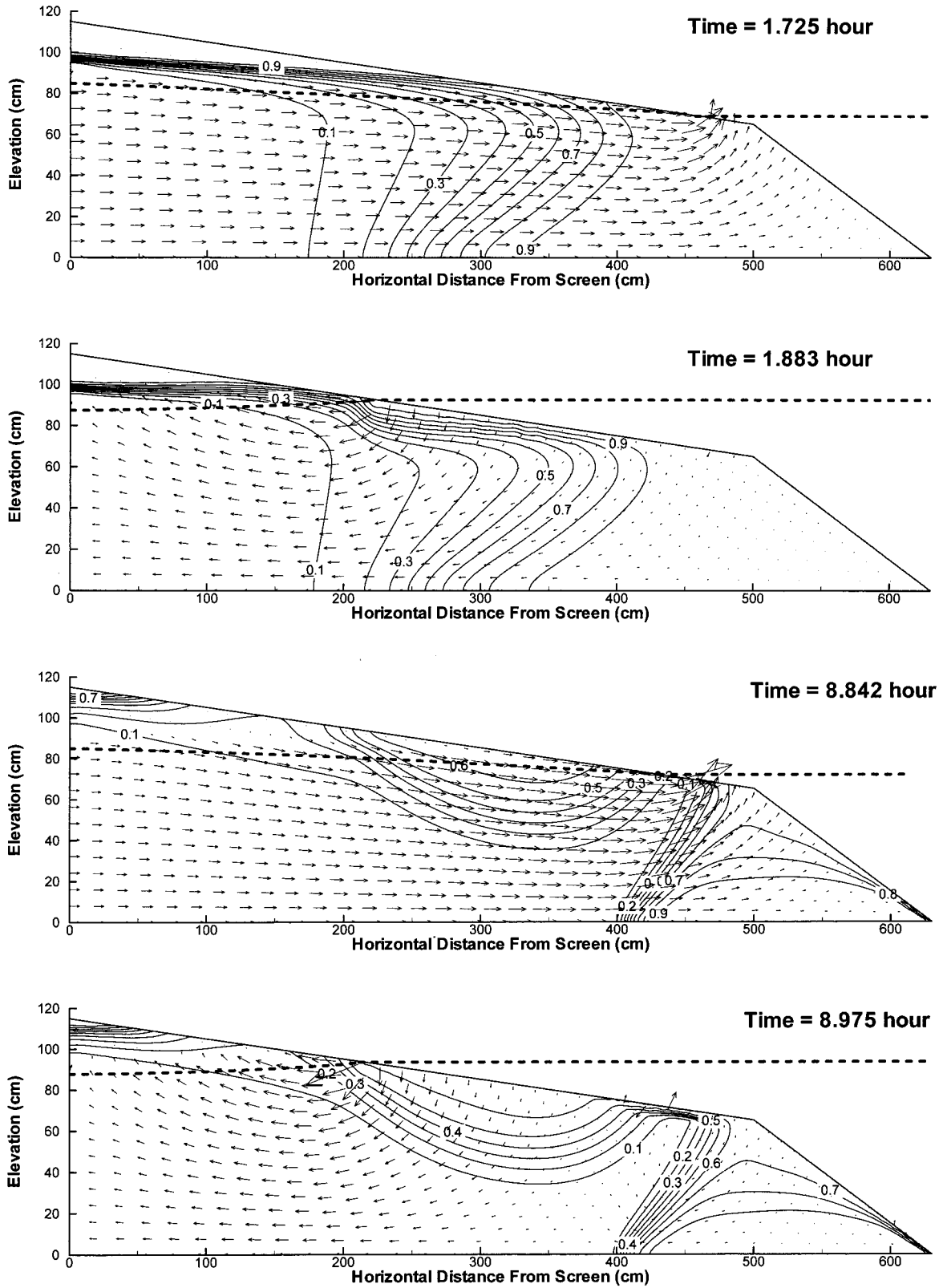
bottom of the tank (in fact, throughout the sand) immediately increased. The reader is reminded that the weight of water solution above the water table does not affect the readings at the PTs, because this weight is carried by capillary forces, whose support is the sand skeleton (the formula of K. Terzaghi [Cedergren, 1967]). The pressure decreased later because of the arrival of the freshwater front, which occurred for  $0.75 \text{ hour} < t < 1.5 \text{ hours}$  (note CM3 and CM4) at PT3, and for  $1.0 \text{ hour} < t < 1.5 \text{ hours}$  (note CM6 and CM9) at PT4.

Figure 6 shows modeling results at times  $t = 1.725$ ,  $t = 1.883$ ,  $t = 8.842$ , and  $t = 8.975$  hours. As in case 1 (Figure 3), these analysis times were selected to show the behavior of the dependent variables in the beach (pressure, concentration, Darcy flux) just before the tidal cycle, at the first high tide, at the last low tide, and at the last high tide. Buoyancy caused the formation of the saltwater wedge at the lower section of the

beach at  $t = 1.725$  hours (Figure 6). As in case 1, the salinity at the beach surface increased under a high tide ( $t = 1.883$  hours, Figure 6). Later, Figure 6 shows a quasi-steady state distribution (cyclic) of salinity in the intertidal zone of the beach. Notice that eventually, two salinity plumes appear in the beach separated by low salinity at the beach surface around  $x = 460 \text{ cm}$  (the separation occurred around  $x = 470 \text{ cm}$  in case 1, Figure 3).

The fluctuating velocities near the beach surface at  $x = 430 \text{ cm}$  (Figure 6,  $t = 8.975$  hours) reflect the inherent instability of a system containing a dense saltwater plume overlying a less dense plume. The reader is referred to Schincariol *et al.* [1997] for an investigation on the gravitational instabilities of dense saltwater plumes in two-dimensional saturated media.

The dense saltwater plume above the capillary fringe ( $t = 2.5$  hours,  $x < 150 \text{ cm}$ ) was stable because capillary forces



**Figure 6.** Salinity and Darcy flux distribution at four different times for case 2 (density-and-viscosity-dependent flow) using the fine grid. The arrows represent the Darcy flux. The dashed lines represent the beach water table and the sea water level.

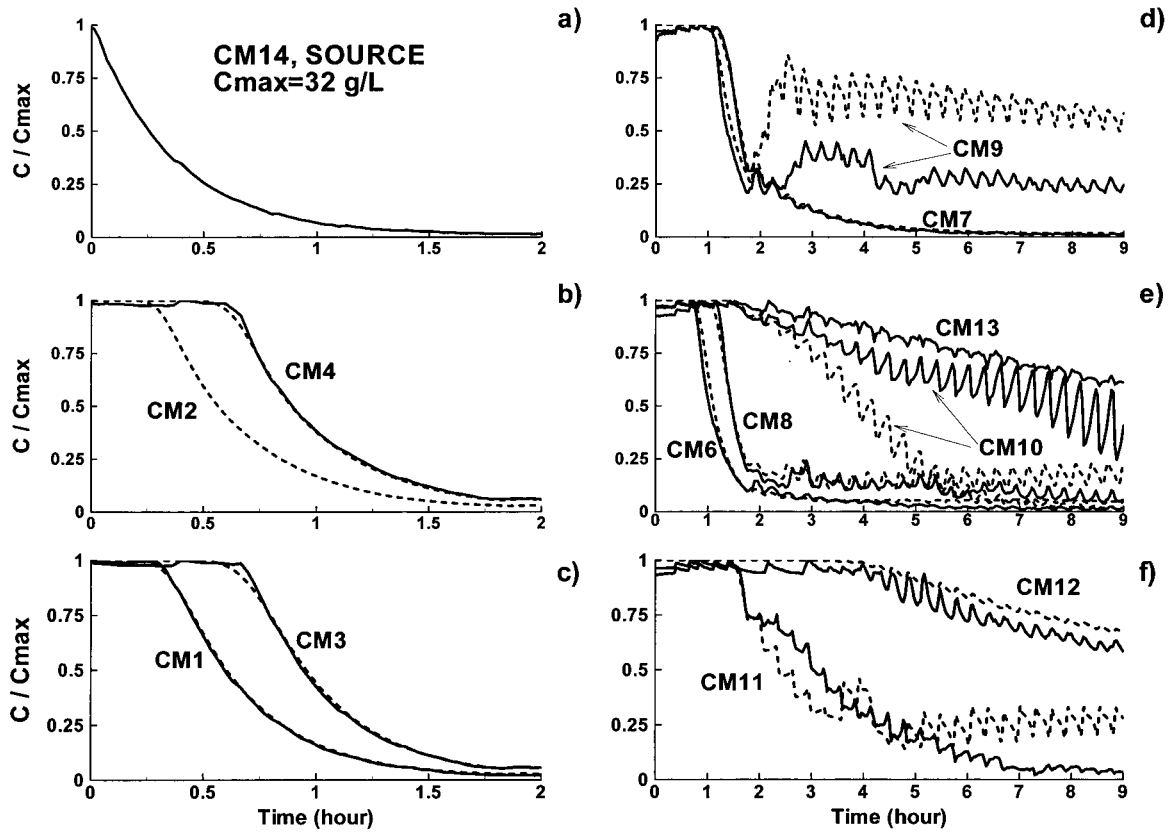


**Figure 7.** Observed and simulated concentrations of case 2 obtained by assuming a density-dependent but isoviscous flow (i.e., salt concentration affects water density but not water viscosity). Fine grid results are shown.

were much larger than buoyancy forces. In other words, the water flow in the unsaturated zone was dictated by the soil moisture, which was very small because of the coarseness of the sand. The low soil moisture resulted in small water flows.

The simulations of case 2 (Figures 4, 5, and 6) represent the realistic situation where the salt concentration affects both water density and viscosity. To assess viscous effects, we conducted a simulation of case 2 where water viscosity was assumed to be unaffected by the salt concentration (i.e., isoviscous assumption). This was done in the MARUN model by setting  $\xi = 0$  in (2). The results obtained from the fine grid simulation are plotted in Figure 7.

By comparing Figure 7 to Figure 5 one notes that in the early part of the experiment ( $t < 1.70$  hours) the fresh water propagated faster in the beach in the isoviscous case in comparison to the viscous case (e.g., CM1, CM3, CM4, and CM11), which is the expected result. However, no major changes in the numerical solution are noted, which supports the common assumption of neglecting viscosity effects when dealing with seawater concentrations (say,  $c \approx 30 \text{ g L}^{-1}$ ) [Galeati *et al.*, 1992; Boufadel *et al.*, 1999a]. This is not typically true when dealing with highly saline water ( $c \approx 300 \text{ g L}^{-1}$ ), where neglecting viscosity effects greatly alters subsurface dynamics [Boufadel *et al.*, 1999b].

## 7. Sensitivity to Parameters

The parameter  $S_f$  was measured at 0.01 [Boufadel *et al.*, 1998; Boufadel, 1998]. The bulk diffusion coefficient  $\tau D_f$  was

set at  $10^{-6} \text{ cm}^2 \text{ s}^{-1}$ . The measured porosity of 0.36 was adopted. The remaining parameters of the beach sand (Table 2) were estimated by visually fitting the model to the data. Although automatic optimization was conducted in conjunction with the MARUN model in a previous work [Boufadel *et al.*, 1998], the long duration of the simulation time in this work prohibited such an approach. Furthermore, because of the high number of sensors used in this study, the “best” fit has a certain degree of subjectivity; the goal of the experiments was to better understand beach hydraulics due to tide and/or buoyancy, with a special attention on the intertidal zone. Therefore the focus was put on fitting the model to the data in the intertidal range without significantly “forcing” the parameters. To a reasonable degree, this was achieved in this study; the parameter values were all in the physically expected range.

The experiment of case 2 was conducted about a week before that of case 1. In between, other experiments were conducted (including ones with waves). This fact and stochastic errors would result in a different parameter set for each experiment. Hence one of the challenging tasks was to select each parameter such that it can represent both experiments. As listed in Table 2, this task was achieved for all parameters with the exception of the saturated hydraulic conductivity, which had to be different between case 1 and case 2, highlighting the major role the saturated hydraulic conductivity plays. Because this is an expected result, no further investigation on the effect of the saturated hydraulic conductivity on beach hydraulics and hydrodynamics is pursued in this work.

### 7.1. Unsaturated Flow Parameters

The fitted values of  $\alpha$  ( $0.125 \text{ cm}^{-1}$ ) and  $n$  (3.0) are close to those obtained by Boufadel *et al.* [1998] ( $\alpha = 0.155 \text{ cm}^{-1}$  and  $n = 3.3$ ), who fitted the MARUN model to water pressure data in the laboratory beach using Bayesian nonlinear optimization. In that work, a sensitivity analysis revealed that the transient water table is highly sensitive to the saturated hydraulic conductivity and  $\alpha$  and almost insensitive to the parameter  $n$ . A similar conclusion was reached by Boufadel *et al.* [1999c], who investigated the effect of unsaturated flow parameters on the location of the steady state water table and on steady state outflows in two-dimensional media. The estimated value of  $n = 3.0$  falls in the high end of  $n$  values reported in the literature [Morel-Seytoux *et al.*, 1996]. This is to be expected because of the uniformity of the sand.

Simulation results obtained with  $n = 1.5$  for both case 1 and case 2 (not shown) were very similar to those reported in Figures 3 and 6, especially at later times. The only difference was in the concentration contours in the unsaturated zone landward of the high tide line, where  $n = 1.5$  resulted in a mild concentration gradient. This is due to the fact that for  $n = 1.5$  the transition between the capillary fringe and the zone above it is smooth with a higher amount of water retained in the unsaturated zone above the capillary fringe in comparison with the  $n = 3.0$  situation [see Boufadel *et al.*, 1998, Figure 4a].

### 7.2. Dispersivities

The estimation of dispersivities is more nebulous because many theoretical and experimental studies have shown that heterogeneity in the subsurface causes dispersivity values to increase with the travel distance (or travel time) from the source [e.g., Gelhar and Axness, 1983; Neuman, 1990; Rajaram and Gelhar, 1995]. The functional relation between the dispersivity and travel distance is still an unresolved issue because the relation depends on how one conceptually models subsurface heterogeneity (e.g., stationary noise [Gelhar and Axness, 1983]; fractal [Molz and Boman, 1993]; or multifractal [Boufadel *et al.*, 2000]). Hence, even if a functional relation between dispersivity and travel distance is assumed, the lack of information on the heterogeneity of the beach and the transient two-dimensional flow in and out of the beach makes assigning a value to the dispersivity based on travel distance an impossible task. For this reason, beach-averaged dispersivities were estimated.

The value 0.75 cm (Table 2) appears appropriate for both cases (Figures 2, 4, and 5). The value of 0.25 cm for the transverse dispersivity results in an  $a_L/a_T$  value of 3 which is smaller than values found in the literature (from 5 to 10 for homogeneous media [Schincariol *et al.*, 1997]). The reason that the transverse dispersivity is large (i.e., the ratio is small) is probably due to the fact that the observed concentration readings were obtained by averaging over the volume of the plexiglass boxes. Simulation results of case 1 and case 2 obtained with  $a_T = 0.1$  cm (not shown) showed a rapid increase of the salinity at CM6 and CM8 in comparison with the results reported in Figure 2 (case 1) and Figure 5 (case 2). The fast increase is attributed to the lack of mixing that would result in dilution of the salt water entering the beach. The long-term results (last low and high tides) were not much different from those reported in Figures 3 and 6.

The sensitivity of the results to the value of the longitudinal dispersivity was investigated by conducting simulations with  $a_L = 3.0$  cm while keeping the remaining parameter at the

values reported in Table 2. Simulation results with  $a_L = 3.0$  cm (not shown) translated the saline water mass downward and seaward. This is attributed to the location of the sources of fresh water and salt water to the beach: The fresh water enters the beach from the landward side, and the salt water enters the beach from the sea side. In comparison with  $a_L = 0.75$  cm (Figures 3 and 6) the value  $a_L = 3.0$  cm resulted in dilution of the water landward of the intertidal zone and increased concentration of the water in the intertidal zone. The effects of dilution appear to be greater when buoyancy effects are present (case 2), which indicates that fresh water passing through the screen propagated upward in the unsaturated zone because of buoyancy effects.

The reason that  $n$  and  $a_L$  do not have major effects on the long-term behavior of the saltwater plume in the intertidal zone is most likely due to “dominating” effects by the sea boundary condition due to the obvious fact that the submerged beach surface constitutes a large geometric boundary.

An important issue in selecting the longitudinal dispersivity is numerical dispersion (i.e., oscillations in the solution [Anderson *et al.*, 1984]), which could result if the grid (or local) Peclet number is larger than 2.0. This implies, when neglecting molecular diffusion, that oscillations in the solution could appear if the longitudinal dispersivity is less than half the distance between nodes within an element. In this work, the maximum value of the Peclet number was at  $x = 0$ , and it took the values  $3.5/0.75 = 4.67$  in the coarse mesh and  $2.2/0.75 = 2.93$  in the fine mesh, but no oscillation in the solutions was observed. Pinder and Gray [1977, p. 163] report oscillation-free solutions for a Peclet number of 5.35. Huyakorn and Pinder [1983, p. 206] argue that in many cases involving nonuniform flow, acceptable numerical solutions are achieved even when the grid Peclet number is as high as 10.

## 8. Nondimensionalization and Scaling

The previous results can be generalized, and, in particular, scaled up, using the dimensionless formulation of Boufadel *et al.* [1998, 1999a]. The approach consists of conducting the following nondimensionalization:  $x^* = x/L$ ,  $z^* = z/L$ ,  $\psi^* = \psi/L$ ,  $K^* = K_{xo}/K_o = K_{zo}/K_o$ ,  $t^* = t/T_o$ , where  $L$  is a characteristic length and  $T_o = L/K_o$ ,  $a_L^* = a_L/L$ ,  $a_T^* = a_T/L$ , and  $\alpha^* = \alpha L$ , where starred quantities are dimensionless. By rewriting (3)–(7) as functions of starred quantities it can be shown [Boufadel *et al.*, 1999a, 1999b] that the hydraulics and hydrodynamics in two domains of different sizes (but geometrically similar) are the same provided the dimensionless quantities above are conserved along with  $n$ ,  $S_r$ , and  $\phi$ . An important result of the dimensionless formulation is that scaling down porous media requires a coarser porous medium in the small-scale system. A detailed methodology for scaling down (or up) physical systems was presented by Boufadel *et al.* [1998, 1999a, 1999b]. Briefly, one selects the ratio of scaling down (say, fivefold) and then the laboratory sand that conserves the value of  $\alpha$  (this is an easy task because it is always possible to find a sand coarser than found in a natural beach). The saturated freshwater hydraulic conductivity of the laboratory sand is measured and used to compute the tidal period in the laboratory setup (the tidal amplitude in the laboratory would be the large-scale tidal amplitude divided by 5). Table 3 lists the properties of a natural beach that could be experimentally simulated by the laboratory setup with the sand properties of case 2.

Scaling the dispersivity values simply by multiplication by a constant is not straightforward because, as discussed in section 7.2, the dispersivities (and in particular the longitudinal dispersivity) increase with both the degree of heterogeneity and the travel distance from source. However, when dealing with beaches, the following considerations must be taken into account: (1) Most beaches are sandy and therefore tend to exhibit a much higher degree of homogeneity than inland aquifers. (2) As shown in this study, water flow and solute transport in the intertidal zone of beaches are highly two dimensional. Therefore the travel time (or distance) is small, and the longitudinal dispersivity should not be viewed as that obtained from water flow occurring parallel to the beach surface but perpendicular to it. Hence the longitudinal dispersivity value of typical natural beaches is probably only a little larger than the value 3.75 cm reported in Table 3. Furthermore, the sensitivity analyses demonstrated that long-term intertidal zone hydrodynamics of a natural beach with  $a_L = 3.0 \text{ cm} \times 5 = 15 \text{ cm}$  (5 is the scale-up factor, Table 3) are not very different from those obtained from the same beach if one assumes  $a_L = 3.75 \text{ cm}$ .

Unless taking extreme values,  $S_r$  and  $\phi$  of sandy beaches do not greatly affect water flow [Boufadel, 1998; Boufadel et al., 1998]. Hence the dimensionless formulation is flexible, allowing for a wide application of the results of the laboratory beach.

## 9. Discussion

Results of this work showed that the saltwater plume for case 1 (no buoyancy effects) occupied a larger area in the beach than that of density-dependent case 2: if one considers the 0.1 isochlor as the edge of the plume. In order to assert that the difference was due to buoyancy effects we investigate two parameters that were different between the two cases: (1) the water level at the sea side and (2) the saturated freshwater hydraulic conductivity.

1. During the tidal action the water level behind the screen (PT1) was the same in case 1 and case 2, but because of difference in density the sea water levels of case 2 were  $\sim 2.5\%$  lower than those of case 1. Because it was thought that the difference in water level affected the salinity distribution, a high-salinity ( $32 \text{ g L}^{-1}$ ) experiment was conducted where the sea hydraulic boundary condition was controlled by a water level gauge instead of PT5, thereby allowing a comparison with case 1 on a water level basis. The results of the experiment were similar to those reported in Figure 6 and are not shown for brevity.

2. One might argue that the larger spreading of the salt-

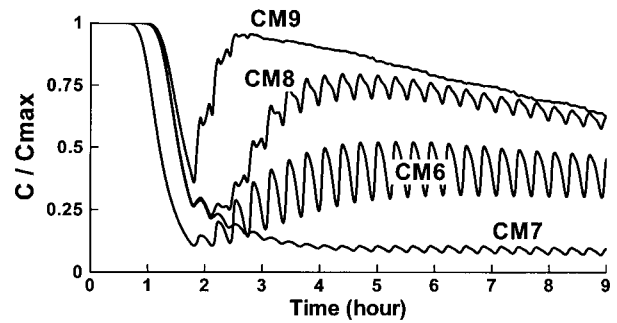


**Figure 8.** Observed and simulated concentrations of case 2 obtained by assuming that the salt has no effect on water density or viscosity. Fine grid results are shown.

water plume in case 1 in comparison with case 2 was due to the fact that the freshwater saturated hydraulic conductivity was different between case 1 ( $0.65 \text{ cm s}^{-1}$ ) and case 2 ( $0.75 \text{ cm s}^{-1}$ ). For this reason, a simulation of case 2 was obtained with  $\varepsilon = 0$  (equation (1)) and  $\xi = 0$  (equation (2)); hence the salt has no effect on water density or viscosity. The results (Figure 8) are similar to those of case 1 (Figure 3) despite the difference in the saturated hydraulic conductivity: Figure 8 shows that the variation of CM9 with time was smooth and the salinity at CM6 and CM8 reached high values, which is unlike the density-and-viscosity-dependent results shown in Figure 5.

It is therefore concluded that buoyancy effects reduced the areal extent of the saltwater plume by opposing the downward movement of the salt water through the beach surface.

## 10. Effect on Bioremediation

Because marine oil spills reach the shore as a thin film floating on the water, the length of the contamination zone (along the length of the beach) is dictated by the minimum and maximum water level in the sea (in the absence of waves). Although the tidal amplitude was constant in this study, the tidal amplitude on natural beaches varies with the position of the moon with respect to the Earth. The maximum tidal amplitude occurs at a full moon (spring tide) while the minimum tidal amplitude occurs at a quarter moon (neap tide). If the tidal amplitude in this study is considered to be occurring at a spring tide, then the bioremediation zone is confined to the intertidal zone. However, if it is considered to be occurring during a neap tide, the bioremediation zone extends beyond the intertidal zone of the laboratory beach in both the seaward and the landward directions. Therefore it is assumed for generality of interpretation that the bioremediation zone occupies all of the laboratory beach surface. On the other hand, common dissolved nutrients are inorganic salts, such as nitrate and phosphate [Venosa et al., 1996; Boufadel et al., 1999d], that do not adsorb to the beach sand. Their concentrations are generally on the order of  $2\text{--}3 \text{ g L}^{-1}$  such that it can be assumed that they do not affect beach hydraulics. These two observations allow application of this work's results to investigate strategies for the application of dissolved nutrients.

The steady state hydraulic boundary conditions showed that a very small water flow occurs seaward of the location where the water table intersects the beach surface (Figures 3 and 6). Therefore only small amounts of nutrients applied landward of or in the intertidal zone of the beach will reach the bioremediation zone seaward of the intersection point. In particular,

**Table 3.** Scale-up of the Case 2 Parameters

| Physical Quantity                      | Case 2 | Natural Beach |
|--|--------|---------------|
| $L$ , cm                               | 630    | 3150          |
| $K_{so}$ , $\text{cm s}^{-1}$          | 0.75   | 0.127         |
| $K_{xq} = K_{zo}$ , $\text{cm s}^{-1}$ | 0.75   | 0.127         |
| $\alpha^{-1}$ , cm                     | 8      | 40            |
| $a_L$ , cm                             | 0.75   | 3.75          |
| $a_T$ , cm                             | 0.25   | 1.25          |
| Tidal amplitude $A$ , cm               | 25     | 125           |
| Tidal period $T$                       | 22 min | 12.25 hours   |
| $\phi$                                 | 0.36   | 0.36          |
| $n$                                    | 1.5    | 1.5           |
| $S_r$                                  | 0.01   | 0.01          |

the contaminated zone seaward of the low neap tide cannot be bioremediated during a neap tide cycle. Figures 3 and 6 show that nutrients applied in fresh water landward of the beach propagate upward in the capillary fringe but do not cross it to reach the unsaturated zone above it. Hence these nutrients would reach the bioremediation zone if the capillary fringe is greater than or equal to the distance between the water table and the bioremediation zone. In other words, bioremediation of the zone landward of the tide level can be achieved by applying nutrients landward of the beach provided that the sand has a large capillary fringe (e.g., a fine-textured sand). It is important to note that the role of the capillary fringe is not limited to nutrient delivery; even if high nutrient concentrations are present in the bioremediation zone, sufficient soil moisture is needed for microbial growth.

Figures 3 and 6 show that nutrients present in the intertidal zone close to the beach surface are driven downward into the beach during a rising tide. Hence maximum oil biodegradation is expected to occur landward of the intersection point of the beach surface with the tide level provided that sufficient nutrients and moisture are present in the bioremediation zone. Although we have noted that successful bioremediation can be achieved if nutrients were applied in a trench landward of a fine-textured beach, these beaches are characterized by a low hydraulic conductivity, which implies that the nutrients might not reach the bioremediation zone before the high tide occurs. Therefore it appears that application of the nutrients onto the beach surface at low tide [Venosa *et al.*, 1996] is the best application strategy. A refinement on the method used by Venosa *et al.* [1996] for coarse beaches would be to apply the nutrient solution intermittently on the beach surface to provide sufficient moisture for microbial growth.

## 11. Conclusions

Two laboratory experiments were conducted to investigate the effects of tides and buoyancy on beach hydraulics in the presence of a seaward groundwater flow due to an elevated regional water table. In the first experiment case 1, the difference in concentration between the salt water at sea and the water of the regional aquifer was small such that it did not engender density gradients. In such a case the salt water acts as a tracer. In the second experiment the difference was  $\sim 32.0 \text{ g L}^{-1}$ , which created a significant density gradient; in this case the regional groundwater is fresh water. The experiments were numerically simulated by the MARUN model [Boufadel *et al.*, 1999a]. The following conclusions can be reached: (1) The long-term experimental and numerical results of both case 1 and case 2 showed that the seawater plume entered the beach from the sea and occupied most of the intertidal zone. The maximum depth of the seawater plume was near the midsection of the intertidal zone, and it decreased near the boundaries of the intertidal zone. When viewed in the context of case 2, these results indicate an inverted salinity distribution with salt water from sea ( $32 \text{ g L}^{-1}$ ) overtopping the freshwater lens. When normalized to the maximum concentration of each case, the depth of the saltwater plume in case 2 was smaller than that of case 1, which is due to the fact that buoyancy gradients opposed the downward movement of salt water from sea. In both cases, water from the regional aquifer moved seaward beneath the seawater in the intertidal zone and pinched out near the low tide mark. (2) Beach hydraulics and hydrodynamics are highly two-dimensional with water entering the beach at

a near-vertical angle and leaving at a near-horizontal angle. (3) Viscosity effects were negligible with respect to density effects for the situations that we considered. (4) Application of the nutrients at the beach surface at low tide appears to be the best application strategy of nutrients.

## Notation

|               |  |
|---------------|--|
| $a_L$         | longitudinal dispersivity.                               |
| $a_T$         | transverse dispersivity.                                 |
| $c$           | salt concentration.                                      |
| $D$           | dispersion tensor.                                       |
| $D_f$         | diffusion coefficient.                                   |
| $k_x$         | horizontal permeability.                                 |
| $k_z$         | vertical permeability.                                   |
| $K_x$         | horizontal freshwater hydraulic conductivity.            |
| $K_z$         | vertical freshwater hydraulic conductivity.              |
| $K_{x0}$      | saturated freshwater horizontal hydraulic conductivity.  |
| $K_{z0}$      | saturated freshwater vertical hydraulic conductivity.    |
| $m, n$        | parameters of the <i>van Genuchten</i> [1980] model.     |
| $q_x$         | horizontal Darcy flux.                                   |
| $q_z$         | vertical Darcy flux.                                     |
| $S$           | saturation ratio.  |
| $S_o$         | elastic storage per unit fluid weight.                   |
| $S_e$         | effective saturation ratio.                              |
| $S_r$         | residual soil saturation.                                |
| $x$           | horizontal coordinate.                                   |
| $z$           | vertical coordinate.                                     |
| $\alpha$      | a parameter of the <i>van Genuchten</i> [1980] model.    |
| $\beta$       | ratio of saltwater density to freshwater density.        |
| $\delta$      | fitting parameter for the viscosity concentration curve. |
| $\varepsilon$ | fitting parameter for the density concentration curve.   |
| $\phi$        | porosity.  |
| $\psi$        | pressure head.   |
| $\tau$        | tortuosity.  |

**Acknowledgments.** This work was supported, in part, by the U.S. Environmental Protection Agency's National Risk Management Research Laboratory, Cincinnati, Ohio, under Cooperative Agreement CR-821029. However, it does not necessarily reflect the views of the agency, and no official endorsement should be inferred. The author acknowledges support from the Department of Civil and Environmental Engineering at the University of Cincinnati.

## References

- Anderson, D. A., J. C. Tannehill, and R. H. Pletcher, *Computational Fluid Mechanics and Heat Transfer*, Hemisphere, New York, 1984.
- Bear, J., *Dynamics of Fluids in Porous Media*, Elsevier Sci., New York, 1972.
- Boufadel, M. C., Nutrient transport in beaches: Effect of tides, waves, and buoyancy, Ph.D. thesis, Dep. of Civ. and Environ. Eng., Univ. of Cincinnati, Cincinnati, Ohio, 1998.
- Boufadel, M. C., M. T. Suidan, and A. D. Venosa, Density-dependent flow in one-dimensional variably-saturated media, *J. Hydrol.*, 202, 280–301, 1997.
- Boufadel, M. C., M. T. Suidan, C. H. Rauch, A. D. Venosa, and P. Biswas, 2-D variably-saturated flow: Physical scaling and Bayesian estimation, *J. Hydrol. Eng.*, 3, 223–231, 1998.
- Boufadel, M. C., M. T. Suidan, and A. D. Venosa, A numerical model for density-and-viscosity-dependent flows in two-dimensional variably-saturated porous media, *J. Contam. Hydrol.*, 37, 1–20, 1999a.
- Boufadel, M. C., M. T. Suidan, and A. D. Venosa, Numerical modeling

- of water flow below dry salt lakes: Effect of capillarity and viscosity, *J. Hydrol.*, *221*, 55–74, 1999b.
- Boufadel, M. C., M. T. Suidan, A. D. Venosa, and M. T. Bowers, Contribution of capillary flow to steady-seepage: Application to trenches and dams, *J. Hydraul. Eng.*, *125*, 286–294, 1999c.
- Boufadel, M. C., P. Reeser, M. T. Suidan, B. A. Wrenn, J. Cheng, X. Du, and A. D. Venosa, Optimal nitrate concentration for the biodegradation of n-heptadecane in a variably-saturated sand column, *Environ. Technol.*, *20*, 191–199, 1999d.
- Boufadel, M. C., S. Lu, F. J. Molz, and D. Lavallee, Multifractal scaling of the intrinsic permeability, *Water Resour. Res.*, in press, 2000.
- Brown, A. C., and A. McLachlan, *Ecology of Sandy Shores*, Elsevier Sci., New York, 1990.
- Cedergren, H. R., *Seepage, Drainage, and Flow Nets*, 489 pp., John Wiley, New York, 1967.
- Celia, M. A., E. T. Bouloutas, and R. L. Zarba, A general mass-conservative numerical solution for the unsaturated flow equation, *Water Resour. Res.*, *26*, 1483–1496, 1990.
- Forkel, C., and M. A. Celia, Numerical simulation of unsaturated flow and contaminant transport with density and viscosity dependence, in *Computational Methods in Water Resources IX*, vol. 2, *Mathematical Modeling in Water Resources*, pp. 351–359, Comput. Mech., Boston, Mass., 1992.
- Frind, E. O., Simulation of long-term transient density-dependent transport in groundwater, *Adv. Water Resour.*, *5*, 73–88, 1982.
- Galeati, G., G. Gambolati, and S. P. Neuman, Coupled and partially coupled Eulerian-Lagrangian model of freshwater-seawater mixing, *Water Resour. Res.*, *28*, 149–165, 1992.
- Gelhar, L. W., and C. L. Axness, Three-dimensional stochastic analysis of macrodispersion in aquifers, *Water Resour. Res.*, *19*, 161–180, 1983.
- Glover, R. E., The pattern of fresh water flow in coastal aquifers, *J. Geophys. Res.*, *64*, 439–475, 1959.
- Henry, H. R., Effects of dispersion on salt encroachment in coastal aquifers, *U.S. Geol. Surv. Water Supply Pap.*, *1613-C*, C71–C84, 1964.
- Huyakorn, P. S., and G. F. Pinder, *Computational methods in subsurface flow*, 473 pp., Academic, San Diego, Calif., 1983.
- Huyakorn, P. S., J. W. Mercer, and D. S. Ward, Saltwater intrusion in aquifers: Development and testing of a three-dimensional finite element model, *Water Resour. Res.*, *23*, 293–312, 1987.
- Merlin, F.-X., C. Chaumery, J. Oudot, R. P. J. Swannell, A. Basseres, C. Dalmazzone, J. Ducreux, K. Lee, and T. Reilly, Bioremediation: Results of the field trials of Landevennec (France), *Proceedings of the 1995 International Oil Spill Conference*, pp. 917–918, Am. Pet. Inst., Washington, D. C., 1995.
- Molz, F. J., and G. K. Boman, A fractal-based stochastic interpolation scheme in subsurface hydrology, *Water Resour. Res.*, *29*, 3769–3774, 1993.
- Morel-Seytoux, H. J., P. D. Meyer, M. Nacache, J. Touma, M. T. van Genuchten, and R. J. Lenhard, Parameter equivalence for the Brooks-Corey and van Genuchten soil characteristics: Preserving the effective capillary drive, *Water Resour. Res.*, *32*, 1251–1258, 1996.
- Neuman, S. P., Saturated-unsaturated seepage by finite elements, *J. Hydrol. Div. Am. Soc. Civ. Eng.*, *12*, 2233–2250, 1973.
- Neuman, S. P., Universal scaling of hydraulic conductivities and dispersivities in geologic media, *Water Resour. Res.*, *26*, 1749–1758, 1990.
- Nielsen, P., Tidal dynamics of the water table in beaches, *Water Resour. Res.*, *26*, 2127–2134, 1990.
- Philip, R. J., Periodic nonlinear diffusion: An integral relation and its physical consequences, *Aust. J. Phys.*, *26*, 513–519, 1973.
- Pinder, G. F., and W. G. Gray, *Finite element simulation in surface and subsurface hydrology*, 294 pp., Academic, San Diego, Calif., 1977.
- Rajaram, H., and L. W. Gelhar, Plume-scale dependent dispersion in aquifers with a wide range of scales of heterogeneity, *Water Resour. Res.*, *31*, 2469–2482, 1995.
- Riedl, R. J., N. Huang, and R. Machan, The subtidal pump: A mechanism of interstitial water exchange by water action, *Mar. Biol.*, *13*, 210–221, 1972.
- Rosenberg, E., R. Legmann, A. Kushmaro, R. Taube, E. Adler, and E. Z. Ron, Petroleum bioremediation: A multiphase problem, *Biodegradation*, *3*, 337–350, 1992.
- Safferman, S. I., Selection of nutrients to enhance biodegradation for the remediation of oil spilled on beaches, *Proceedings of the 1991 International Oil Spill Conference*, pp. 571–576, Am. Pet. Inst., Washington, D. C., 1991.
- Schincariol, R. A., F. W. Schwartz, and C. A. Mendoza, Instability in variable density flows: Stability and sensitivity analyses for homogeneous and heterogeneous media, *Water Resour. Res.*, *33*, 31–41, 1997.
- van Genuchten, M. T., A closed-form equation for predicting the hydraulic conductivity of unsaturated soils, *Soil Sci. Soc. Am. J.*, *44*, 892–898, 1980.
- Venosa, A. D., M. T. Suidan, B. A. Wrenn, K. L. Strohmeier, J. R. Haines, B. L. Eberhart, D. King, and E. Holder, Bioremediation of an experimental oil spill on the shoreline of Delaware Bay, *Environ. Sci. Technol.*, *30*, 1764–1775, 1996.
- Weast, R. C. (Ed.), *CRC Handbook of Chemistry and Physics*, 63rd ed., CRC Press, Boca Raton, Fla., 1983.
- Wise, W. B., O. Guven, F. J. Molz, and S. C. McCutcheon, Nutrient retention time in high-permeability, oil-fouled beach, *J. Environ. Eng.*, *120*, 1361–1379, 1994.
- Xue, X., C. Xie, and J. Wu, A three-dimensional miscible transport model for seawater intrusion in China, *Water Resour. Res.*, *31*, 903–912, 1995.

---

M. C. Boufadel, Department of Civil and Environmental Engineering, Temple University, 1947 North 12th Street, Philadelphia, PA 19122. (boufadel@astro.temple.edu)

(Received November 24, 1999; revised April 19, 2000; accepted May 17, 2000.)

